Janus SEGPHOS: Integrating Persistent Photogenic Radicaloids with Multiple Circularly Polarized Doublet Radiance and Long-persistent Triplet Phosphorescence

Bo Yang[1†], Suqiong Yan[1†], Shirong Ban[1], Yuan Zhang[1], Hui Ma[1], Fanda Feng[1], and Wei Huang[1,2*]

Organic phosphors integrating circularly polarized persistent luminescence (CPPL) across the visible range are prevalent for applications in optical information encryption, bioimaging, and 3D display, but the pursuit of color-tunable CPPL in a single-component organics remains a formidable task. Herein, via in-suit photo-implanting radical ion-pairs into axial chiral crystals, we present and elucidate an unprecedented double-module decay strategy to achieve a colorful CPPL through a combination of stable triplet emission from neutral diphosphine and doublet radiance from photogenic radicals in an exclusive crystalline framework. Owing to the photoactivation-dependent doublet radiance component and an inherent triplet phosphorescence in the asymmetric environment, the CPL vision can be regulated by altering the photoactivation and observation time window, allowing colorful glow tuning from blue and orange to delayed green emission. Mechanism studies reveal that this asymmetric electron migration environment and hybrid *n*-π*, π-π* instincts serve an afterglow and radical radiance at ambient conditions. Moreover, we demonstrate the applications of colorful CPPL for displays and encryptions via manipulation of both excitation and observation time.

Circularly polarized persistent luminescence refers to the selective polarization emission nature in luminophores. The right or left-handedness of circularly polarized light is observed for specifically extended emission after the shutdown of external excitation light in the chiral phosphor isomers (Scheme 1a).[1–12] This long-lived emission extension is associated with the spin-forbidden transition of intersystem crossing (ISC) and limited energy delivery, leading to an insufficient phosphorescence in pure organic phosphors because of small spin-orbit coupling parameters and unstable triplet excited states.[13–20] Nevertheless, organic room-temperature phosphorescence (RTP) has still attracted growing dedication in recent decade due to its lower fabrication price and intricate excited-state emission, which bring out potential application areas in optical information anticounterfeiting, sensor, bioimaging, 3D display, and spintronics.[21–26] In terms of this, one of the most important topics is how to improve the diversity of optical information, such as color, lifetime, and even optics polarization state. That above-described diversity can boost encrypted data complexity and storage capacity.[27,28]

Up to now, despite the significant progress of acquiring colorful RTP in organic phosphors, where the cocrystallization,[15,17] host-guest co-assembly,[29,30] molecular polymerization,[5,10] supramolecular polymerization,[31,32] metal-organic framework (MOF)/covalent organic framework (COF) incarceration [33–35] have been developed. However, the structural breakthrough and mechanistic unveiling of colorfully emissive crystals with hybrid singlet, doublet, triplet excited states, and non-invasive stimulate manipulation is an intriguing but challenging topic in the field of single component organic room-temperature phosphorescence (ORTP),[16] not to mention integrating color-tunable circularly polarized persistent luminescence (Scheme 1b).[3]

Notably, recent works demonstrate multicolor emission can be obtained in excitation wavelength-dependent single-component molecular crystals under different excitations due to the formation of multiple emitting centers under ambient conditions;[6,36] or driven by Anti-Kasha's rule,[37] or triggered by ground/excited-state conformational change.[38–41] However, the morphologic packing construction needs to be changed in some cases after applying external mechanical or thermal stimulus. Distinctly, the non-invasive photostimulation and crystal structure preservation are favorable for information display and operation feasibility in optical encryption.

In this context, we can get an inspired realization concept of multicolor CPPL under different photoactivations by orthotopically constructing multiple emitting roles and decay channels in exclusively molecular crystals.[42–48] That is to say, the new emitting molecular composition in situ arose after photostimulation, but the supramolecular crystal framework is still maintained (Scheme 1c, 1d). Therefore, this Janus balance integrates both pristine emissive centers and subsequently photogenic luminescence components. Recently, we have found a platform to produce the transient P(III) radicaloids from electron-rich diphosphines (*i.e.* SEGPHOS) by photoactivation or Mn(III)-mediated C-P bond activation in solution. The following annulated phosphonium product ([6b]$^+$) forms stable triplet excited states because of the intrinsic *n*-π*, π-π* feature in

[1]State Key Laboratory of Coordination Chemistry, Nanjing National Laboratory of Microstructures, School of Chemistry and Chemical Engineering, Nanjing University, Nanjing 210093, P. R. China. E-mail: whuang@nju. edu.cn

[2]Shenzhen Research Institute of Nanjing University, Shenzhen 51805, P. R. China

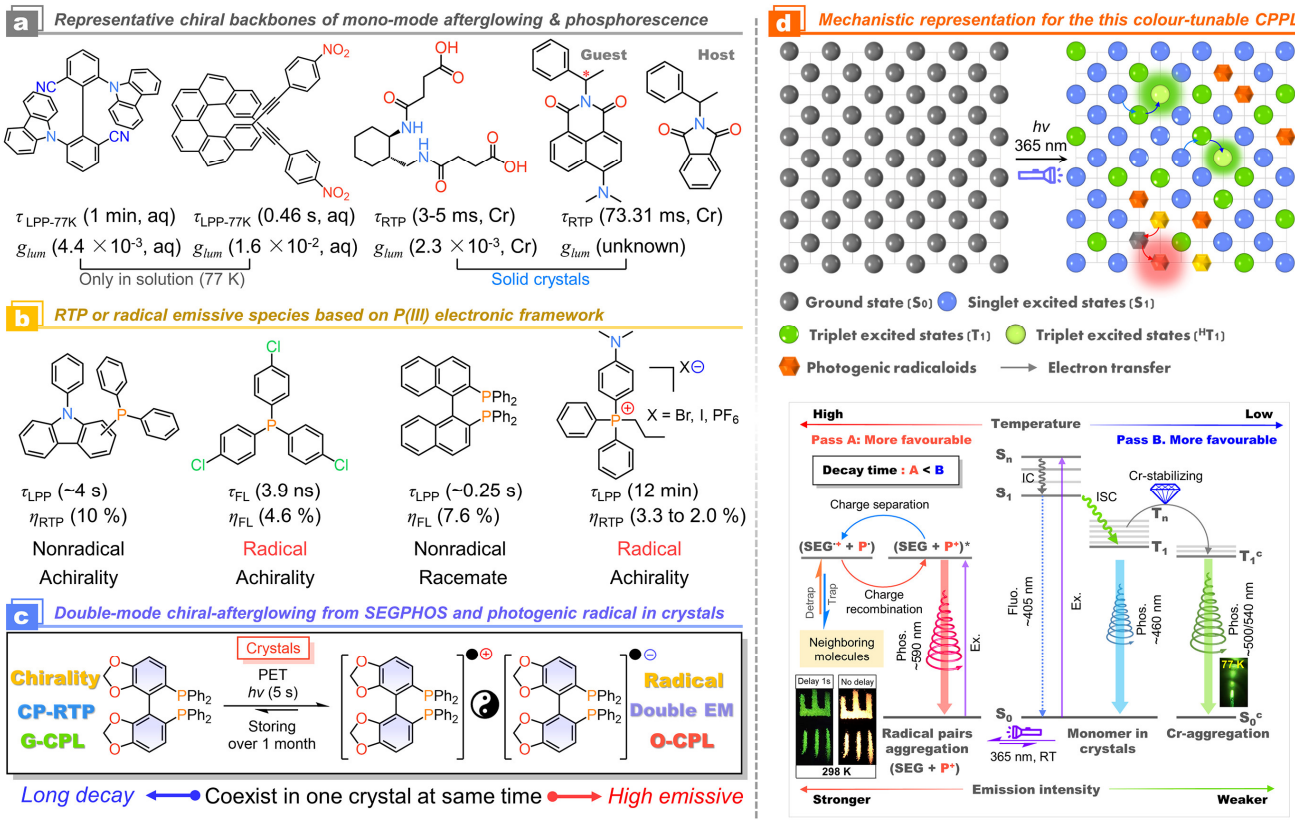

Scheme 1. Conceptual design of single-component color-tunable RTP or radical emission. (a) Chiral single-component organics, their chemical configurations, and key phosphorescence behaviors. (b) RTP and radical emissive species based on organic P(III) compounds and their emission behaviors. (c) Chemical structures and double decay strategy from SEGPHOS and its photogenic radical in crystals in this work. (d) Schematic energy transfer processes and mechanism of fluorescence (Fluo.) and phosphorescence (Phos.) occurring in the SEGPHOS crystal following photoactivation and excitation (Ex).

4,4′-bibenzo[d][1,3]dioxole, favoring an effective ISC, triplet population, and triplet energy transfer to $[MnCl_4]^{2-}$ in single crystals.[49] We speculate that this SEGPHOS can provide a potential platform with both stable triplet excited states and persistent photogenic radicaloids capability by crystal engineering.

The lone pair electrons on dual P(III)-atoms and heteroatoms might experience an intramolecular *n*-π* electronic transfer to enhance ISC or through-space charge transfer (TSCT) to promote electron escape. To validate this blueprint, we focus on three kinds of O-atom embedded diphosphines containing four locked or unlocked O-atoms (Figure 1a), which could not only accelerate the ISC rate to boost triplet excitons but also shape lavish non-covalent intermolecular interactions (NCIs) and crystal morphology to restrict molecular motion for triplet phosphorescence in crystals, even stabilize the latter formed photogenic radicaloids. Consequently, the molecules and crystals featuring axial chiral configurations and asymmetry should facilitate the formation of a chiral coupling environment and charge separation, which provides the multi-mode chiral doublet and triplet in favor of circularly polarized luminescence (CPL) and CPPL with multiple color-tunable from short-life deep blue, orange to long-lived green persistent luminescence and high dissymmetry factor of 3.7 × 10^{-3}. Finally, this photoactivation correlative emission color has also been utilized to establish time and chiral-dependent information encryption. These findings provide a new principle for the development of chiral phosphorescent materials and stable radical emitters with dynamically non-invasive controllability.

Results and discussion

Economical and controllable scale-up of material synthesis is the crucial impetus for application evolution. Herein, these diphosphines are extraordinary and cheap ligands, that could be easily purchased from many commercially available sources. This ligand synthesis and generalization in asymmetric catalysis can be traced back to different breakthroughs from Saito, Genet, Schmid, and co-workers, et. al.[50–53] Although the original samples of SEGPHOS also display both photochromism and RTP phenomenons further purification verification might be necessary to rule out the induced artifact of trace impurity.[54] Hence, three high-purity diphosphines (~99% purity, 99% *ee*) were purchased from a commercial source and further purified by multiple recrystallizations (three times) in chloroform and hexane mixture before investigation, getting a satisfying chemical and crystalline phase purity according to high-performance liquid chromatography (HPLC, >99.9 % purity), NMR, single crystals X-ray diffraction (SCXRD), and powder-XRD profiles (Figures, S1−S28). In addition, this reproducibility is also supported

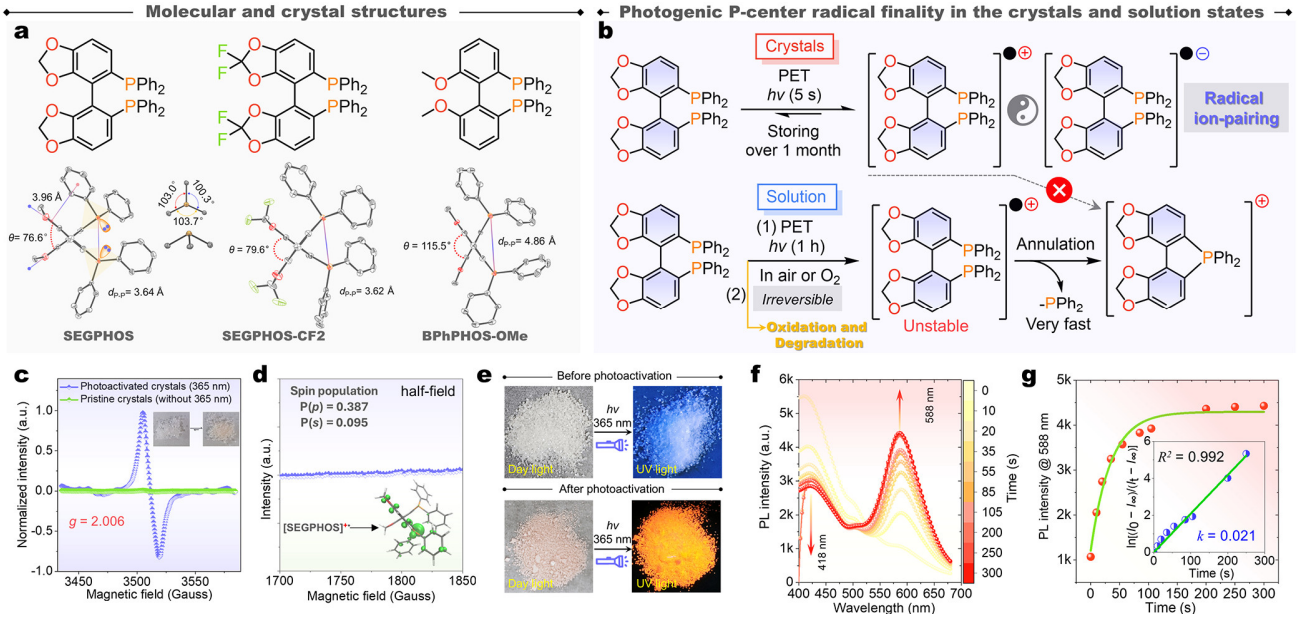

Figure 1. Solid-state structures and photochromism performance and photogenic radical mechanism. (a) Molecular and single-crystal structures (thermal ellipsoids set at the 50%) of three targeted diphosphines. (b) The reasonable generation and conversion passway of active photogenic radicals of SEGPHOS. (c) EPR spectra of (*R*)-SEGPHOS before and after photoactivation (with 365 nm flashlight for 1 min, 4.8 W cm^{-2}). (d) Corresponding EPR spectra at half-field and spin-density populations of $[SEGPHOS]^{+\bullet}$ (its anionic radical partner was given in ESI). The DFT calculation is performed at UB3LYP/6-31G(d) level. (e) The observations of color and emission changes of (*R*)-SEGPHOS single crystals upon UV-activating. (f) Photoactivation time-dependent photoluminescence spectra (PL spectra, the optical power density of flashlight is 4.8 W cm^{-2}). (g) Emission intensities change at radical emission peaks of 588 nm. Calculated responsivity rates and corresponding kinetic parameters (inset) of (*R*)-SEGPHOS crystals according to the first-order reaction kinetics equation $ln[(I_0 - I_\infty)/(I_t - I_\infty)]=kt$, Where the *k* is responsivity rate constant, R^2 is the fitting coefficient, I_∞ and I_0 is saturation emission and initial intensities, respectively. I_t is the dynamic intensities at different time stages.

by different commercial SEGPHOS sources with identical optical properties (Figure S41). Pure SEGPHOS oxide (potential impurity in impure SEGPHOS) lacks photochromism and the RTP phenomenon and has a larger optical band gap (Figures S40c, S40d).

In the beginning, the unnatural photochromism of crystals SEGPHOS at ambient conditions after 365 nm flashlight irradiation aroused our vigilance and attention. As shown in Figure 1e, the pristine crystals of SEGPHOS are colorless under indoor light but change to slight pink after a few seconds of irradiation (Figure 1c). The gradation of pink color and a new orange emission both increases until saturation with add of exposure duration to UV light. To quantitatively understand these photochromism behaviors, the photosensitive ability of this crystal is investigated by monitoring the variations in emission spectra at the whole visible bands under continuous 365 nm UV flashlight irradiation with a power density of 4.8 W cm^{-2}. According to the first-order reaction kinetic model of $ln[(I_0 - I_\infty)/(I_t - I_\infty)]=kt$,[41,55] the responsivity rate constant (k) is determined as 0.021 s^{-1} (details see ESI), in which the enhancement index I_∞/I_0 of 4.18 with corresponding saturated photoactivation time of ~4 min is obtained (Figure 1f, 1g). Moreover, this kinetic process is highly power density-dependent as found truth of sluggish saturation progress under in situ illumination from the fluorescence spectrum exciting light (Figure S42). In addition, excitation-wavelength-related tests of SEGPHOS crystals indicate that successful photoactivation emerged under UV light irritation ranging from ~330 to 410 nm and the best excitation wavelength of the activation is ~365 nm (Figure 2e).

Subsequently, structure and spectrum measurements are performed to unravel the governing mechanisms behind the photochromism and emergent emission of crystals. The UV–vis absorption of SEGPHOS film exhibits an absorption onset at around 400 nm, which is consistent with its colorless crystalline film. However, the colorless film gradually turns slightly pink upon UV irradiation (365 nm) for 10 seconds, and three new absorption bands are centered at 410, 520, and 700 nm (Figure 2a). The NMR, IR, and SCXRD profiles of the completely photoactivated sample match well with its pristine unactivated ones (Figures S4–S8, S25, S40, Tables S1, S5–S8). These results demonstrate the photogeneration of trace species is only stable in crystals, and these new emitters with such narrow optical gaps might be derived from radical forms instead of simple molecular isomerization, oxidation, or polymorphism transition.[43,44] As anticipated, electron paramagnetic resonance (EPR) provides a strong single-electron signal with a *g*-value of 2.006 in photoactivated crystals but no signal is detected for the pristine sample without UV exposure (Figure 1c). Importantly, the photoactivated crystals are quite persistent

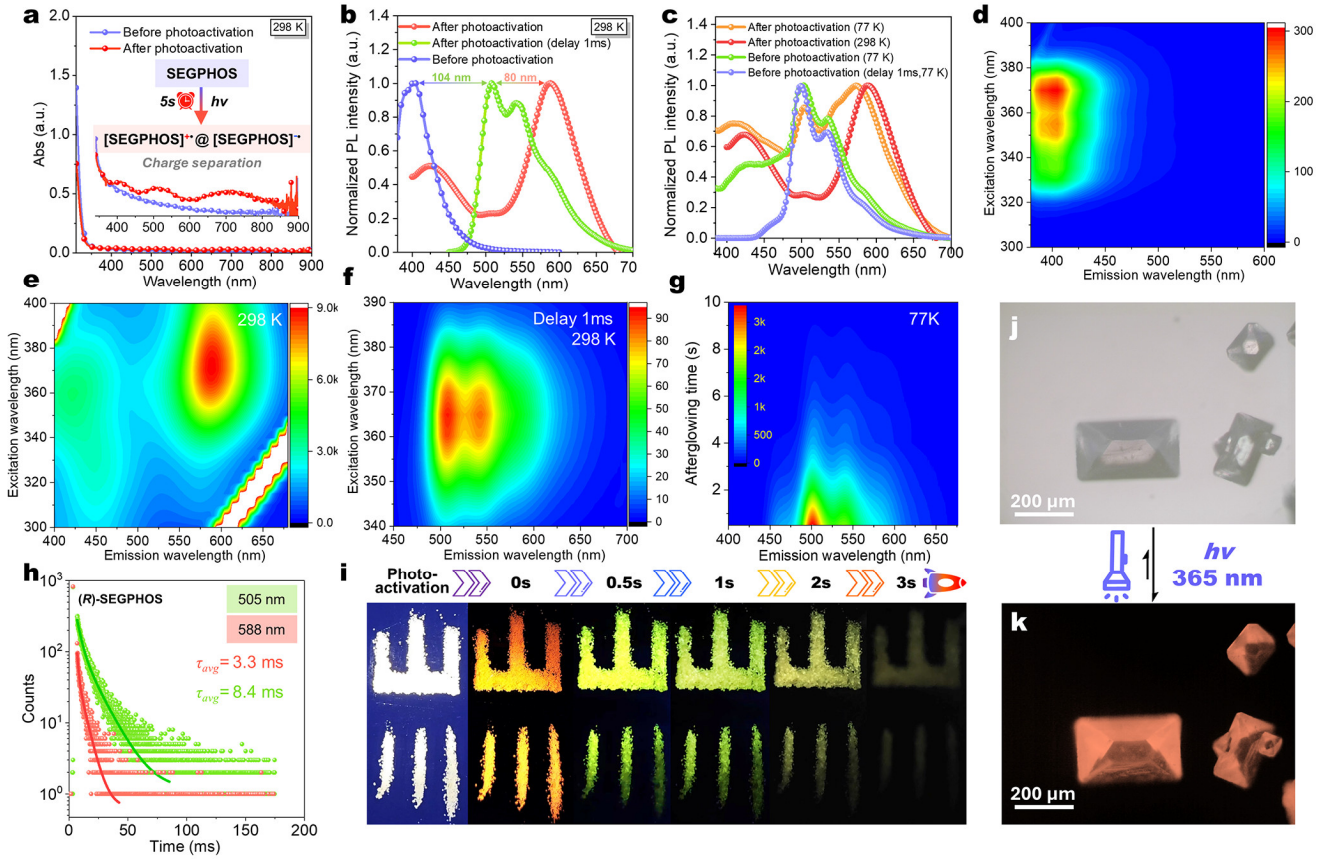

Figure 2. Photophysical properties of SEGPHOS. (a) UV-vis spectra of (*R*)-SEGPHOS films under ambient conditions. (b) PL and delay PL spectra of (*R*)-SEGPHOS before and after complete photoactivation at 298 K. (c) PL and delay PL spectra of (*R*)-SEGPHOS before and after complete photoactivation at 298 K and 77 K. (d) PL mapping spectra and intensity profiles of unactivated (*R*)-SEGPHOS crtstals excited at different wavelengths (the Ex. slit is seted as smaller 2 nm and scan speed is seted as higher 2400 nm min^{-1} to suppress photo-activation). (e) PL mapping spectra of photoactivated (*R*)-SEGPHOS crtstals excited at different wavelengths (298 K) and (f) Delay PL mapping spectra of photoactivated (*R*)-SEGPHOS crtstals excited at different wavelengths (298 K, delay 1ms). (g) Delayed emission spectra mapping of photoactivated (*R*)-SEGPHOS at 77 K (excited at 365 nm). (j, k) Photographs of (*R*)-SEGPHOS single crystals taken under a 365 nm lamp on and off at ambient conditions. (h) Time-resolved emission intensity at 590 nm and 505 nm of photoactivated (*R*)-SEGPHOS crystals upon excitation by 365 nm (298 K). (i) Representative photographs of ultralong RTP observed in the (*R*)-SEGPHOS crstals at ambient conditions.

and can be maintained for a few weeks before being deactivated to the original state under ambient conditions (Figure S39), suggesting the presence of persistent photogenic radicaloids must be responsible for photochromism and emergent orange-red radiance. The absent signal of photogenic radicaloids at half-field suggests a single radical charter via the loss of one electron at the *p*-orbit of certain P-atom rather than biradicals with two unpaired electrons.[56] This fact is supported by an electron-rich character on P-atoms and the highest electron transfer difference from HOMO to LUMO on P-atoms (Figure S60). Certainly, the spin population analysis of the cationic $[SEGPHOS]^{+\bullet}$ partner displays the dominant component on one P-atom *p*-orbit ($P_{(p)}$=0.387) and trifling delocalization on the dioxole unit (Figures 1d, S61). This exposed radical reactivity suffers radical degradation in solution but persistent existence in protecting crystalline framework (Figures S21−S25).[49] The unstable radical feature has also been detected by additional UV-vis absorption cross 400−900 nm in a $Cu(OTf)_2$-mediated reaction (Figure S38). It is worth noting that the generation and stability of this radical are extremely sensitive to the molecular packing model as corroborated by inexistent photochromism and EPR activities for SEGPHOS-CF2 and BPhPHOS-OMe (Figures S39c, S39d, vide infra).

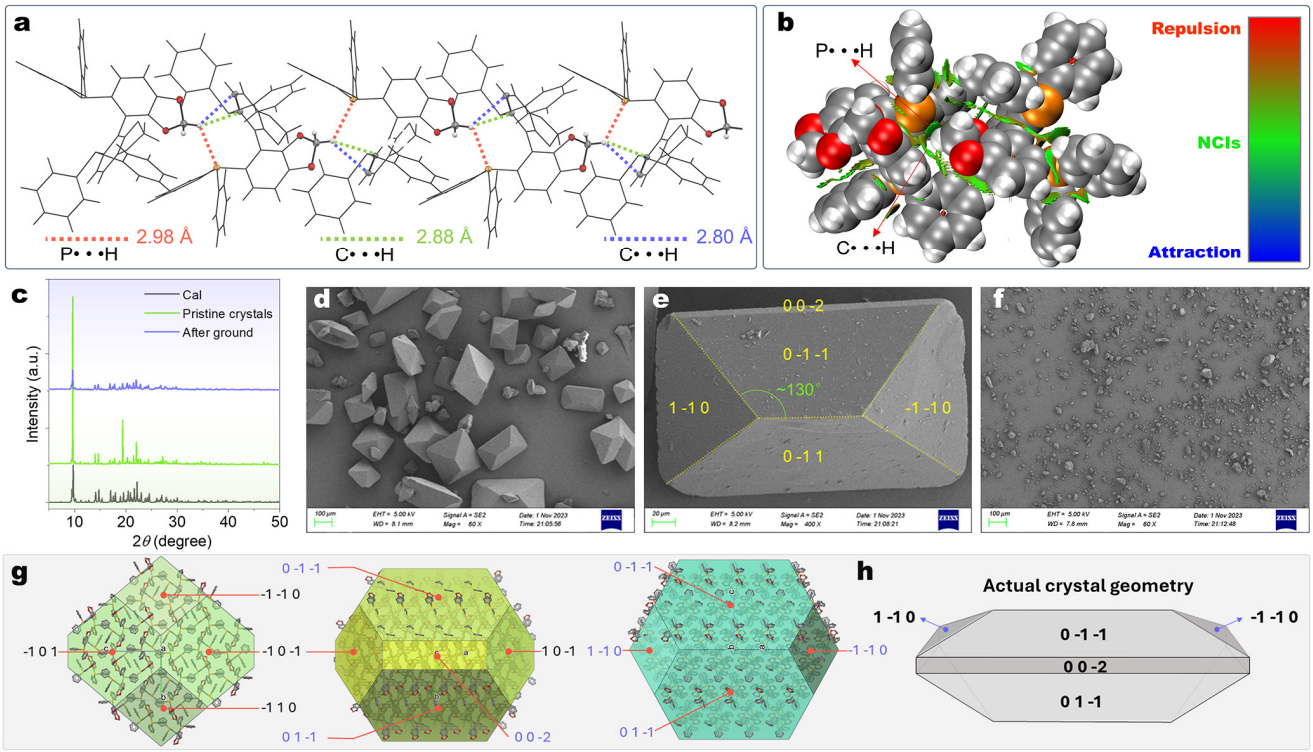

Figure 3. Single crystal and morphology analyses of polyhedral (*R*)-SEGPHOS. (a) Crystal paking and intermolecular interactions of (*R*)-SEGPHOS. (b) Reduced density gradient (RDG) isosurfaces of paking dimer (*s* = 0.6 au). (c) Simulative XRD and PXRD of pristine crystals and grinding sample. (d) Field-emission SEM (FE-SEM) images of (*R*)-SEGPHOS crystals and (e) the enlarged morphology of one crystal. (f) FE-SEM image of grinding crystals. (g) The 3D model of (*R*)-SEGPHOS and the predicted 3D geometry on the basis of BFDH morphology. (h) The actual crystal geometry and lattice plane of (*R*)-SEGPHOS crystals.

Expectantly, the unsensitized crystals only emit very weak blue fluorescence at 405 nm with a short decay of 1.37 ns (Figures 2b, 2d, S46d), but the second long-persistent yellow-green luminescence was observed from the uniform SEGPHOS single crystal under ambient conditions after the removal of the 365 nm UV lamp, which is regardless of whether activated or not for crystals (Figures 2i, S44). For the photoactivated sample, the original orange luminescence peak (586 nm) was near annihilated and turned to a yellow-green color as the delay time changed from 0 to 1 ms (Figure 2e, 2f), where the later RTP process three multiple emission peaks at 509, 540, and 586 nm with the long lifetimes of 8.4 ms (505 nm), 3.3 ms (586 nm) (Figure 2c, 2h, video S1). However, the strongest 586 nm emission also undergoes a very fast decay of 5.63 ns, leading to a blue-shift vision and degeneration during RTP progress (Figures S44f, S46a). These results demonstrate the photoactivation-dependent nature of the short-lived doublet fluorescence and photoactivation-independent triplet RTP in these emissive crystals under ambient conditions. TD-DFT simulation of absorption and emission spectra for radical $[SEGPHOS]^{+\bullet}$ and $[SEGPHOS]^{-\bullet}$ pairs have been calculated. Consequently, the isolated absorption spectra of radical cation and anion show different strongest peaks at 633 and 1640 nm (Figure S64b), which correlate well with the experimental measurements and suggest the absorption contribution of the radical residue in crystals. Generally, the strongest doublet emission of the radical cation is present in contrast to the quenched character of the radical anion due to internal conversion.[44,57,58] Therefore, the long-wavelength emission of 586 nm is made by the radical cation part but the strongest RTP band originated from the pristine SEGPHOS matrix (Figure S45).

We further attempt to measure the excitation-dependent emission spectra of the SEGPHOS. As shown in Figure 2d–2f, there are no dependencies could be found for the long-persistent luminescence but the photogenic radical emission relates to excitation-wavelegth. The former multiple RTP splits might be caused by different decay channels between the distinct triplet states (n-T_1) and ground (S_0) states of the compact stacking in neighboring molecules for crystals.[4] Based on low-temperature delay spectra of monomeric SEGPHOS in DCM and PMMA film at 77 K (Figure S49), four hypochromatic shift peaks appeared at 452, 478, 488 nm which do not completely agree well with the experimental data for crystals at 77 K (498, 534, and 573 nm, Figure 2c). Notably, compared with the RTP in the SEGPHOS crystal at 298 K, the slight blue-shift phosphorescence (~7 nm) involves improved phosphorescence efficiency and afterglow time (7.9% and ~7s) at 77 K due to restricting molecular thermal motion (Figure 2g, S48). However, the emission intensities of the DCM solution and doped PMMA film are extremely weak at 77 K (Φ<0.1%). The radical emission is also disappeared Therefore, we believe that strong. intermolecular interactions along the neighboring molecules play a crucial

role in realizing enhanced crystal phosphorescence even stabilizing radical lifetime.[57,59]

To disclose the mechanisms of both persistent photogenic radical radiance and long-persistent luminescence. We further test our hypothesis using two similar diphosphines with slight differences, where the bridged H-atoms on dioxoles are replaced by F-atoms to retain the molecular configuration and electronic structure (SEGPHOS-CF2). Another contrast BPhPHOS-OMe has two open methoxy groups to rebuild stereoscopic and electronic configuration (Figure 1a). For spectrum observation and EPR measurements of SEGPHOS-CF2 and BPhPHOS-OMe crystals, no photoactivated radical emission and EPR signal are found after UV irradiation (Figures S39, S51, S52). In view of single crystal diffraction data and uniform dodecahedron morphology, the enantiomeric (*R*)-SEGPHOS and (*S*)-SEGPHOS show a mirrored stereochemical configuration with almost the same crystallographic and structural parameters (Figures S29−S36, Tables S1−S3). Interestingly, (*R*)-SEGPHOS crystallizes in the chiral $P2_12_12_1$ space group with a regular dodecahedron prism. Although the experimental angles between crystal faces are in accordance with theoretical values. The crystal shape slightly deviates tetrakaidecahedron from BFDH theory (Figure 3g),[60] arising from the distinct growth speed between the ideal crystal and the actual crystal. This partly slow growth of crystal face families {(-1 0 -1) (-1 0 1), (1 0 1), (1 0 -1)} and fast progress of {(-1 1 0), (-1 -1 0), (1 1 0), (1 -1 0)} facilitates D_{2h} symmetry of the dodecahedron (Figure S35). Thus, the actual dodecahedron geometry of the crystals results from an integration of intrinsic homochiral features and differential growth rates.[61,62] Based on the sight of crystallographic molecular structure, SEGPHOS and its fluoro-analogs SEGPHOS-CF2 have similar spatial configuration and bonding parameters, in which the SEGPHOS and SEGPHOS-CF2 exhibit the dihedral angles (θ) of 76.6 and 79.6° between two 4,4′-bibenzo[d][1,3]dioxole parts, respectively. The trigonal P(III)-centers are distorted due to subtle noncovalent interaction effects (NCIs) in both intermolecular and intramolecular disturbances (Figures 1a, S34), *i.e.* the centroid contact could be noticed with 3.96 Å between phenyl and dioxole (Figure 1a). The axial chiral backbone bears an intramolecular P-P distance ($d_{P\text{-}P}$) of 3.64 Å and 3.62 Å in SEGPHOS and SEGPHOS-CF2. Meanwhile, the asymmetric CH_2-bridge faces the same upperside in (*R*)-SEGPHOS but the reverse underside in (*S*)-SEGPHOS (Figure S31). This key point facilitates the loss of local C_2 molecular symmetry, that also proven by two isolated ^{1}H NMR signals at 5.03, and 5.66 ppm of methylenes (Figure S25). That above-described ^{1}H NMR split is absent in BPhPHOS-OMe because of the free rotation of unlocked methoxyls and the structure holds a perfect C_2 symmetry in solution at 298 K (Figure S15). On the other hand, the DFT simulative monomer structure of (*R*)-SEGPHOS has a clear difference in geometrical parameters but the same C_1 symmetry. Since the structure cast off the intermolecular NCIs and tight packing, the DFT-optimized (*R*)-SEGPHOS displays a large $d_{P\text{-}P}$ (4.69 Å) and dihedral angle (θ=107.5°), resulting in a poor antioxidation with molecular oxygen in solution (Figures S26, S35). Consequently, photo-induced cyclization, oxidation, and complex degradation have been confirmed in solution. The cyclization could be promoted and complex degradation could be restrained, via add of a protonic reaction environment (Figure S21−S26).

Further electronic structure analysis of asymmetric (*R*)-SEGPHOS shows that the HOMO adopts an asymmetric electronic population on one 4,4′-bibenzo[d][1,3]dioxole unit, which is probably beneficial for the exciton escape through the electron transfer mechanism in molecular scale (Figure S61a).[44] However, this nature is not enough to stabilize radicals with such a long lifetime. As shown in Figure 3a, the repeatedly homodirectional dimers are linked by a 1-D chain (4,4′-bibenzo[d][1,3]dioxole facing PPh_2 fragment) with triplex P···H (2.98 Å) and C···H (2.80−2.88 Å) NCIs, and the DFT computational HOMO and LUMO profiles of crystal dimer and trimer suggest unambiguous electron separation between two/three molecules (Figures 4b, S54c, S54d). This reasonable donor-acceptor (D-A) orientation and stacking reinforces electronic migration and hopping between adjacent molecules, endowing a fast photogenic radical rate, ultra-long stability, and excellent radical emission. In contrast, (*S*)-SEGPHOS-CF2 adopts a distinct architecture, and the molecular unit approaches the ideal C_2 symmetry (Figures 1a, S34), which produces a consistent HOMO/LUMO at the whole monomer level (Figures S61b). Their closer dimer adopts an antiparallel stacking (4,4′-bibenzo[d][1,3]dioxole facing another one), which can not process electronic migration to form photogenic radicals due to an inappropriate local D-A migration channel. Like the SEGPHOS-CF2, (*R*)-BPhPHOS-OMe owns a better C_2 symmetry, enlarged $d_{P\text{-}P}$ (4.86 Å), and dihedral angle (θ=115.5°). Therefore, no radical trace is found in EPR and emission spectra measurements (Figures S39d, S52). In fact, the spin density distribution of radical $[SEGPHOS]^{+\bullet}$ inherits an asymmetry feature of SEGPHOS (Figure 1d). This huge influence of electronic structure would caused by subtle asymmetry in molecular and supramolecular dimensionality.[12,8] For the first radical emission process, the one asymmetric SEGPHOS suffers photo-excitation, yielding an excited state. The electron subsequently migrates to nearby molecules via the photoinduced electron transfer (PET) in the compact D-A aggregate network, getting the emissive cation radicals. In this continuous excitation, the prompt geminate recombination produced a short but strong fluorescence at 586 nm (τ_{avg}: 5.63 ns), but the small number of excitons would undergo possible escape and hop across neighboring molecules (Figure 4b, Scheme 1d). Finally, the diffused electrons will recombine with holes resulting in weakly delayed RTP at the same 586 nm (τ_{avg}: 3.3 ms).[57,63]

These dynamic emissions could be changed by the freeze, photoactivation, and altered observation time. Especially for triplet emission of the SEGPHOS matrix, freeze suppresses nonradiative deactivation, stabilizes intermolecular electronic coupling and asymmetric molecular configuration, and even protects the triplet exciton from atmospheric oxygen quenching. Accordingly, an extremely inferior phosphorescence is detected for (*S*)-SEGPHOS-CF2 and (*R*)-BPhPHOS-OMe at 77 K. In

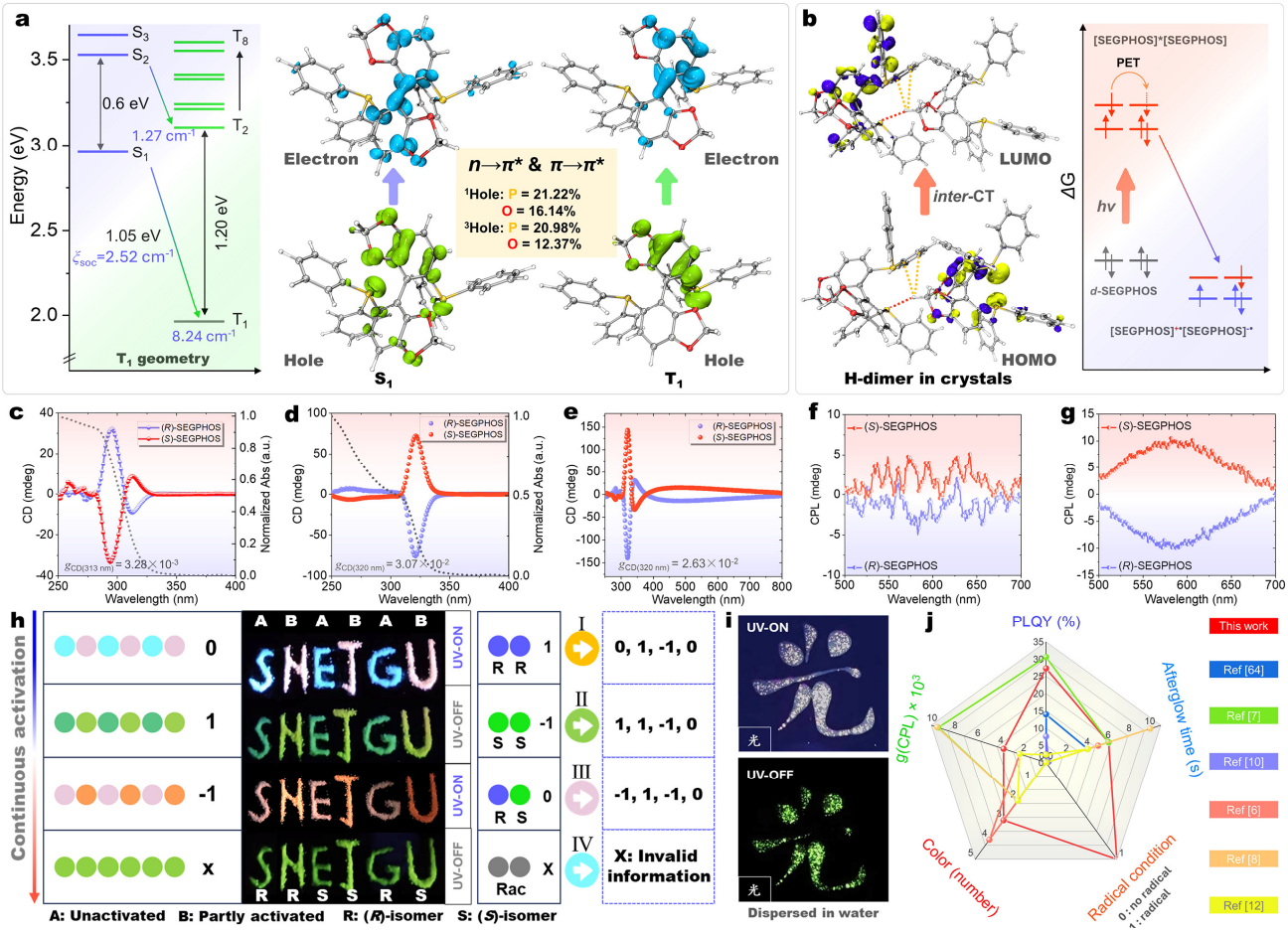

Figure 4. Theoretical calculation analyses and chiroptical properties. The applications in multiple color displays and multiple information encryption under ambient conditions. (a) TD-DFT calculated energy diagram and SOC coefficient (ξ_{soc}) for monomeric (*R*)-SEGPHOS at the T_1-geometry. Electron-hole analyses and orbits components of S_1 and T_1 states. (b) Kohn–Sham of HOMO and LUMO for H-bonding dimer (based on crystal). Schematic electron separation of SEGPHOS and formation photogenic radicaloids. (c, d) ECD spectra of SEGPHOS enantiomer in solution (1.03×10^{-3} M) and solid films under ambient conditions. (e) ECD spectra of SEGPHOS films after photoactivation. (f) CPL spectra of pristine SEGPHOS crystals and (g) after photoactivation (excited at 365 nm). (h) Illustration of multidimensional information encryption using the chiral crystals (*S*)-SEGPHOS and (*R*)-SEGPHOS with different activation stage. (i) Photographs of (*R*)-SEGPHOS crystals (dropwise coating into chinese word '光:light') before and after turning off the 365 nm lamp under dispersed water onditions (active for 20 seconds). (j) Properties comparison for P(III)-based RTP or chiral RTP materials.

contrast, the enantiomeric SEGPHOS outputs a strong long-persistent green phosphorescence even to shine the Dewar flask in darkness for a few seconds (Figure S48, video S2). Remarkably, triplet radiation has gotten more quantum earnings compared to radical fluorescence channels at a low temperature. The intensity ratio of I_{505}/I_{590} (0.854, 77 K) is greatly larger than that of I_{505}/I_{590} (0.286, 298 K), which is improved threefold. Thus the apparent color of lighting changes from orange to plum color (Figures 1c, S48d). Time-dependent density functional theory (TD-DFT) calculations are carried out to penetrate the possible origin of this second persistent RTP of the channel of SEGPHOS. The calculated energy levels between the singlet and triplet states as well as the molecular orbitals alongside the electronic transitions are presented in Figure 4a. The first singlet excitation transfer (S_1) and triplet states (T_1) of the (*R*)-SEGPHOS are all hybrid electronic states with both *n*–*π** and *π*–*π** characters, where P and O-atoms devote a high hole component of 21.22% (P) and 16.14% (O), respectively. These results indicate an appropriate ISC process between the hybrid S_n state and triplet T_n (Figures 4a, S57), which usually generates improved spin-orbit coupling (SOC) values for efficient ISC and ultralong afterglow lifetime according to EI-Sayed's rule.[64,65] There is only one triplet T_1 below the S_1 states for at T_1/S_1-geometries, indicating monotonous ISC channels ($\xi_{soc}\{S_1–T_1\}$=2.52 cm^{-1}, Figures 4a, S56), but many plausible ISC channels in the S_0-/crystal-geometries increase to 10. These cases also have typical *n*–*π** and *π*–*π** characters (Figures S53–S55). In consideration of multiple splits (77 K, ~460, 509, 540 nm) of phosphorescence in crystals and peak positions in solution (77 K, 452, 478, and 488 nm), the molecule configuration might more proceed with the eclectic excited state backbone at rigid condition (77 K and crystals), endowing multiple ISC channels from S_n to T_n.[66,67] It is worth noting that the lowest emission

energy level of crystals (540 nm, 2.3 eV) is quite less than those of solution (488 nm, 2.54 eV). This huge difference must be caused by the lower triplet (T_n') via H-bonding and other NCIs stabilization in dimers (Scheme 1d, T_1'-dimer : 3.17 eV *vs* T_1-Cr : 3.38 eV, Figures S53, S54).[4,36] To ensure this crystallization-induced protection effect, both the first radical emission pathway of $[SEGPHOS]^{+\bullet}$ component and the second RTP channel are seriously degraded upon gently grinding because of loose part crystallinity and crush morphology (Figures 3c, S37, S50, video S3). This fact corroborates the significance of the crystalline state and regular morphology where the pyknotic crystal packing and smaller specific surface protect the photogenic radicals from water and atmospheric oxygen erosion, and also stabilize the excited electronic state for long-persistent luminescence (Figure 4i).

To disclose circularly polarized luminescence (CPL) and CPPL performance SEGPHOS, the electronic circular dichroism (CD) and CPL spectra of pristine and photoactivated (*S*)-SEGPHOS and (*R*)-SEGPHOS spectra are investigated (Figures 4c–4g, S65–S66). Pristine samples in DCM and solid states resolve an approximate couple-splitting slightly at 306 (DCM), 309 nm (solid films), and ultraviolet absorption band (Figure 4a, 4b). However, the concentration-independent $|g_{CD}|$ measurements point out the enhanced value of 3.07×10^{-2} of solid films compared with that of solutions (3.28×10^{-3}). Moreover, slightly red-shift absorption ~6 nm is noticed owing to NCIs in solid. This boosted $|g_{CD}|$ with 9.3 times is ascribed to the chiral coupling from the inherent asymmetry and different molecular configurations of n–π* and π–π* transitions and chiral lattice (Figures S53–S56).[68,69] Most significantly, the CD of photoactivated samples not only inherits the pristine SEGPHOS but also generates a new radical absorb across the whole visible area. That follows deexcitation to pump out a strong doublet CPL with $|g_{CPL}|$ of $\sim 3.7 \times 10^{-3}$ at 586 nm (Figures 4g). In contrast, no or extremely weak CPL emerged in nonactivated samples (Figure 4f). This represents the first discovery of dynamic CPL from photogenic radicaloids up to now.[70–73] Furthermore, the intense CPPL around 500 nm with $|g_{CPPL}|$ of $\sim 2.1 \times 10^{-3}$ is detected at the low temperature, where the crystals are encapsulated in a clear liquid nitrogen chamber at 77 K (Figure S66).

On the basis of the activation time-dependent CPL and long-persistent luminescence feature of these unprecedented single-crystal phosphors. We further demonstrate their potential applications for multicolor visual and chiral encryption of a tunable activation condition. Different letters with diverse photoactivation degrees and stereochemical configurations from 5 to 20 s are designed through a simple coating operation (Figure 4h, 'SEG' abbreviates SEGPHOS, 'NJU' abbreviates Nanjing University). The initial letters emit alternated colors of sky blue and plum (code: 0) under UV light and then evolve into green and yellow-green colors (code: 1) after shutdown of UV light. With further photoactivation, the luminescence image turns to plum and orange (code: -1). Finally, this delayed emission transforms into a saturated yellow-green color (invalid code). Based on the consideration of chiral-associated CPL, the multilevel encryption codes could be defined in "SGEPHOS" by using the chiral (*S*)-SEGPHOS, (*R*)-SEGPHOS, and their racemic mixture, respectively. These source codes are highly dependent on activation time and the information is destroyed after overactivation, representing a Snapchat decode model. Benefiting from good resistance to oxygen and moisture of this electroneutral structure and dense structure, these emissive crystals could be used in water (Figure 4i). As a result, this work manifests the first reliable concept for realizing persistent photogenic radicals with doublet CPL and triplet CPPL.

Conclusion

In conclusion, we have reported the first concept of a double-model decay strategy featuring color-tunable CPL from blue to orange and long-persistent radiance in single-component molecular crystals, which is realized by cascading open-shelled radical emitter center and closed-shell matrix in the Janus SEGPHOS crystals. Experiments and calculations demonstrate that the manipulation of molecular and supermolecular symmetries in crystals is responsible for the tunable n–π* and π–π* characters, photogenic radicals, and triplet emission. Thus, this investigation not only affords a fundamental design principle for achieving chiral multicolor emissions in single-component molecular crystals, but also affirms a reliable concept for developing an accessible platform for multicolor displays, multidimensional chiral anti-counterfeiting, and the prospective radical stereochemistry development of doublet OLEDs.[70,71]

Accession codes

CCDC numbers 2310286−2310289 contain the supplementary crystallographic data for this paper. These data can be obtained free of charge via www.ccdc.cam.ac.uk/data_request/cif, or by emailing data_request@ccdc.cam.ac.uk, or by contacting The Cambridge Crystallographic Data Centre, 12 Union Road, Cambridge CB2 1EZ, UK; fax: +44 1223 336033.

Data availability statement

The data that support the findings of this study are available from ESI or the corresponding author upon reasonable request.

Conflict of interest

The authors declare no conflict of interest.

Acknowledgements

This research was supported by the National Natural Science Foundation of China (No. 21871133), the Natural Science Foundation of Jiangsu Province (No. BK20211146), and the Science, Technology, and Innovation Commission of Shenzhen Municipality (No. JCYJ20180307153251975) for financial support.

Author contributions

W. H. supervised the project and revised the manuscript. B. Y. conducted the research design, property studies, and paper preparation. S.Q.Y. performed the crystallography collections and experimental results discussion. X.X.X. developed the theoretical approach and interpreted the photophysical outcome. All authors discussed the research results and contributed to the paper.

References

(1) Liu, J.; Song, Z.-P.; Wei, J.; Wu, J.-J.; Wang, M.-Z.; Li, J.-G.; Ma, Y.; Li, B.-X.; Lu, Y.-Q.; Zhao, Q. Circularly Polarized Organic Ultralong Room-Temperature Phosphorescence with A High Dissymmetry Factor in Chiral Helical Superstructures. *Adv. Mater.* **2023**, *n/a*, 2306834.

(2) Kabe, R.; Adachi, C. Organic Long Persistent Luminescence. *Nature* **2017**, *550*, 384–387.

(3) Huang, Z.; He, Z.; Ding, B.; Tian, H.; Ma, X. Photoprogrammable Circularly Polarized Phosphorescence Switching of Chiral Helical Polyacetylene Thin Films. *Nat. Commun.* **2022**, *13*, 1–8.

(4) Li, H.; Gu, J.; Wang, Z.; Wang, J.; He, F.; Li, P.; Tao, Y.; Li, H.; Xie, G.; Huang, W.; Zheng, C.; Chen, R. Single-Component Color-Tunable Circularly Polarized Organic Afterglow through Chiral Clusterization. *Nat. Commun.* **2022**, *13*, 1–8.

(5) Gu, L.; Ye, W.; Liang, X.; Lv, A.; Ma, H.; Singh, M.; Jia, W.; Shen, Z.; Guo, Y.; Gao, Y.; Chen, H.; Wang, D.; Wu, Y.; Liu, J.; Wang, H.; Zheng, Y. X.; An, Z.; Huang, W.; Zhao, Y. Circularly Polarized Organic Room Temperature Phosphorescence from Amorphous Copolymers. *J. Am. Chem. Soc.* **2021**, *143*, 18527–18535.

(6) Nie, F.; Wang, K. Z.; Yan, D. Supramolecular Glasses with Color-Tunable Circularly Polarized Afterglow through Evaporation-Induced Self-Assembly of Chiral Metal–Organic Complexes. *Nat. Commun.* **2023**, *14*, 1654.

(7) Zhang, D. W.; Li, M.; Chen, C. F. Axially Chiral Materials Exhibiting Blue-Emissive Ultralong Organic Phosphorescence and Intense Circularly Polarized Luminescence. *Sci. China Mater.* **2023**, *66*, 4030–4036.

(8) Wu, X.; Huang, C. Y.; Chen, D. G.; Liu, D.; Wu, C.; Chou, K. J.; Zhang, B.; Wang, Y.; Liu, Y.; Li, E. Y.; Zhu, W.; Chou, P. T. Exploiting Racemism Enhanced Organic Room-Temperature Phosphorescence to Demonstrate Wallach's Rule in the Lighting Chiral Chromophores. *Nat. Commun.* **2020**, *11*, 1–10.

(9) Kais Dhbaibi, Pierpaolo Morgante, Nicolas Vanthuyne, Jochen Autschbach, L. F.; Crassous, J. Low-Temperature Luminescence in Organic Helicenes: Singlet versus Triplet State Circularly Polarized Emission. *J. Phys. Chem. Lett.* **2023**, *14*, 1073−1081.

(10) Hirata, S.; Vacha, M. Circularly Polarized Persistent Room-Temperature Phosphorescence from Metal-Free Chiral Aromatics in Air. *J. Phys. Chem. Lett.* **2016**, *7*, 1539–1545.

(11) Satyam J, J. E.; Santosh K, M. K.; Thilagar, Y. I. and P. T. Crystallization Induced Room-Temperature Phosphorescence and Chiral Photoluminescence Properties of Phosphoramides. *Chem. Sci.* **2022**, *13*, 5893–5901.

(12) Chen, B.; Huang, W.; Zhang, G. Observation of Chiral-Selective Room-Temperature Phosphorescence Enhancement via Chirality-Dependent Energy Transfer. *Nat. Commun.* **2023**, *14*, 1–8.

(13) Kenry; Chen, C.; Liu, B. Enhancing the Performance of Pure Organic Room-Temperature Phosphorescent Luminophores. *Nat. Commun.* **2019**, *10*, 1–15.

(14) Yang, J.; Fang, M.; Li, Z. Stimulus-Responsive Room Temperature Phosphorescence Materials: Internal Mechanism, Design Strategy, and Potential Application. *Accounts Mater. Res.* **2021**, *2*, 644–654.

(15) Nishimura, N.; Lin, Z.; Jinnai, K.; Kabe, R.; Adachi, C. Many Exciplex Systems Exhibit Organic Long-Persistent Luminescence. *Adv. Funct. Mater.* **2020**, *30*, 1–6.

(16) Sun, H.; Shen, S.; Zhu, L. Photo-Stimuli-Responsive Organic Room-Temperature Phosphorescent Materials. *ACS Mater. Lett.* **2022**, *4*, 1599–1615.

(17) Jinnai, K.; Kabe, R.; Lin, Z.; Adachi, C. Organic Long-Persistent Luminescence Stimulated by Visible Light in p-Type Systems Based on Organic Photoredox Catalyst Dopants. *Nat. Mater.* **2022**, *21*, 338–344.

(18) Liu, Z.; Tian, Y.; Yang, J.; Li, A.; Wang, Y.; Ren, J.; Fang, M.; Tang, B. Z.; Li, Z. Direct Demonstration of Triplet Excimer in Purely Organic Room Temperature Phosphorescence through Rational Molecular Design. *Light Sci. Appl.* **2022**, *11*.

(19) Zhou, Q.; Yang, C.; Zhao, Y. Dynamic Organic Room-Temperature Phosphorescent Systems. *Chem* **2023**, *9*, 2446–2480.

(20) Gao, H.; Ma, X. Recent Progress on Pure Organic Room Temperature Phosphorescent Polymers. *Aggregate* **2021**, *2*, 1–13.

(21) Zhang, M.; Guo, Q.; Li, Z.; Zhou, Y.; Zhao, S.; Tong, Z.; Wang, Y.; Li, G.; Jin, S.; Zhu, M.; Zhuang, T.; Yu, S. H. Processable Circularly Polarized Luminescence Material Enables Flexible Stereoscopic 3D Imaging. *Sci. Adv.* **2023**, *9*, eadi9944.

(22) Li, H.; Li, H.; Wang, W.; Tao, Y.; Wang, S.; Yang, Q.; Jiang, Y.; Zheng, C.; Huang, W.; Chen, R. Stimuli-Responsive Circularly Polarized Organic Ultralong Room Temperature Phosphorescence. *Angew. Chem. Int. Ed.* **2020**, *59*, 4756–4762.

(23) Liu, Y.; Xing, P. Circularly Polarized Light Responsive Materials: Design Strategies and Applications. *Adv. Mater.* **2023**, *2300968*, 1–22.

(24) Buck, J. T.; Boudreau, A. M.; DeCarmine, A.; Wilson, R. W.; Hampsey, J.; Mani, T. Spin-Allowed Transitions Control the Formation of Triplet Excited States in Orthogonal Donor-Acceptor Dyads. *Chem* **2019**, *5*, 138–155.

(25) Huang, A.; Fan, Y.; Wang, K.; Wang, Z.; Wang, X.; Chang, K.; Gao, Y.; Chen, M.; Li, Q.; Li, Z. Organic Persistent RTP Crystals: From Brittle to Flexible by Tunable Self-Partitioned Molecular Packing. *Adv. Mater.* **2023**, *35*, 1–9.

(26) Kim, Y. H.; Zhai, Y.; Lu, H.; Pan, X.; Xiao, C.; Gaulding, E. A.; Harvey, S. P.; Berry, J. J.; Vardeny, Z. V.; Luther, J. M.; Beard, M. C. Chiral-Induced Spin Selectivity Enables a Room-Temperature Spin Light-Emitting Diode. *Science* **2021**, *371*, 1129–1133.

(27) Guo, Q.; Zhang, M.; Tong, Z.; Zhao, S.; Zhou, Y.; Wang, Y.; Jin, S.; Zhang, J.; Yao, H. Bin; Zhu, M.; Zhuang, T. Multimodal-Responsive Circularly Polarized Luminescence Security Materials. *J. Am. Chem. Soc.* **2023**, *145*, 4246–4253.

(28) Wang, C.; Liu, L.; Wang, J.; Yan, Y. Electrochemically Switchable Circularly Polarized Photoluminescence within Self-Assembled Conducting Polymer Helical Microfibers. *J. Am. Chem. Soc.* **2022**, *144*, 19714–19718.

(29) Li, D.; Lu, F.; Wang, J.; Hu, W.; Cao, X. M.; Ma, X.; Tian, H. Amorphous Metal-Free Roomerature Phosphorescent Small Molecules with Multicolor Photoluminescence via a Host-Guest and Dual-Emission Strategy. *J. Am. Chem. Soc.* **2018**, *140*, 1916–1923.

(30) Li, D.; Liu, Z.; Fang, M.; Yang, J.; Tang, B. Z.; Li, Z. Ultralong Room-Temperature Phosphorescence with Second-Level Lifetime in Water Based on Cyclodextrin Supramolecular Assembly. *ACS Nano* **2023**, *17*, 12895–12902.

(31) Gao, L.; Huang, J.; Qu, L.; Chen, X.; Zhu, Y.; Li, C.; Tian, Q.; Zhao, Y.; Yang, C. Stepwise Taming of Triplet Excitons via Multiple Confinements in Intrinsic Polymers for Long-Lived Room-Temperature Phosphorescence. *Nat. Commun.* **2023**, *14*, 1–9.

(32) Ye, W.; Wang, Y.; Cao, T.; Meng, H.; Wang, C.; Hu, B.; Gao, Z.; Wang, C. Respiration-Responsive Colorful Room-Temperature Phosphorescent Materials and Assembly-Induced Phosphorescence Enhancement Strategies. *Small* **2023**, *19*, 1–9.

(33) Liu, H.; Ye, W.; Mu, Y.; Ma, H.; Lv, A.; Han, S.; Shi, H.; Li, J.; An, Z.; Wang, G.; Huang, W. Highly Efficient Blue Phosphorescence from Pillar-Layer MOFs by Ligand Functionalization. *Adv. Mater.* **2022**, *34*, 1–7.

(34) Yu, Q.; Zhang, J.; Lam, J. W. Y.; Yang, D.; Sun, J.; Tang, B. Z. Tunable Room Temperature Phosphorescence in Heavy-Atom-Free Metal–Organic Frameworks by Ligand Functionalization. *ACS Mater. Lett.* **2023**, 2691–2699.

(35) Zhu, Y. Q.; Wang, X. H.; Wu, M. X. Intriguing Room Temperature Phosphorescence in Crystalline Porous Organic Frameworks. *Adv. Funct. Mater.* **2023**, *2308096*, 1–18.

(36) Gu, L.; Shi, H.; Bian, L.; Gu, M.; Ling, K.; Wang, X.; Ma, H.; Cai, S.; Ning, W.; Fu, L.; Wang, H.; Wang, S.; Gao, Y.; Yao, W.; Huo, F.; Tao, Y.; An, Z.; Liu, X.; Huang, W. Colour-Tunable Ultra-Long Organic Phosphorescence of a Single-Component Molecular Crystal. *Nat. Photonics* **2019**, *13*, 406–411.

(37) Li, J.; Li, X.; Wang, G.; Wang, X.; Wu, M.; Liu, J.; Zhang, K. A Direct Observation of Up-Converted Room-Temperature Phosphorescence in an Anti-Kasha Dopant-Matrix System. *Nat. Commun.* **2023**, *14*.

(38) Chen, Z.; Chen, X.; Ma, D.; Mao, Z.; Zhao, J.; Chi, Z. Synergetic Conformational Regulations in Ground and Excited States for Realizing Stimulus-Responsive and Wide-Tuning Room-Temperature Phosphorescence. *J. Am. Chem. Soc.* **2023**, *145*, 16748–16759.

(39) Man, Z.; Lv, Z.; Xu, Z.; He, J.; Liao, Q.; Yang, Y.; Yao, J.; Fu, H. Host Surface-Induced Excitation Wavelength-Dependent Organic Afterglow. *J. Am. Chem. Soc.* **2023**, *145*, 13392–13399.
(40) Tao, Y.; Liu, C.; Xiang, Y.; Wang, Z.; Xue, X.; Li, P.; Li, H.; Xie, G.; Huang, W.; Chen, R. Resonance-Induced Stimuli-Responsive Capacity Modulation of Organic Ultralong Room Temperature Phosphorescence. *J. Am. Chem. Soc.* **2022**, *144*, 6946–6953.
(41) Tao, Y.; Chen, R.; Li, H.; Yuan, J.; Wan, Y.; Jiang, H.; Chen, C.; Si, Y.; Zheng, C.; Yang, B.; Xing, G.; Huang, W. Resonance-Activated Spin-Flipping for Efficient Organic Ultralong Room-Temperature Phosphorescence. *Adv. Mater.* **2018**, *30*, 1–8.
(42) Li, P. X.; Xie, Z. X.; Jin, A. P.; Li, J.; Guo, G. C. A New Photochromic Gd-MOF with Photoswitchable Bluish-White to Greenish-Yellow Emission Based on Electron Transfer. *Chem. Commun.* **2020**, *56*, 14689–14692.
(43) Tang, C.; Song, L.; Zhou, K.; Ren, P.; Zhao, E.; He, Z. Manipulating D-A Interaction to Achieve Stable Photoinduced Organic Radicals in Triphenylphosphine Crystals. *Chem. Sci.* **2023**, *14*, 1871–1877.
(44) Zhao, X.; Gong, J.; Alam, P.; Ma, C.; Wang, Y.; Guo, J.; Zeng, Z.; He, Z.; Sung, H. H. Y.; Williams, I. D.; Wong, K. S.; Chen, S.; Lam, J. W. Y.; Zhao, Z.; Tang, B. Z. A Simple Approach to Achieve Organic Radicals with Unusual Solid-State Emission and Persistent Stability. *CCS Chem.* **2022**, *4*, 1912–1920.
(45) Jin, J. M.; Chen, W. C.; Tan, J. H.; Li, Y.; Mu, Y.; Zhu, Z. L.; Cao, C.; Ji, S.; Hu, D.; Huo, Y.; Zhang, H. L.; Lee, C. S. Photo-Controllable Luminescence from Radicals Leading to Ratiometric Emission Switching via Dynamic Intermolecular Coupling. *Angew. Chem. Int. Ed.* **2023**, *62*.
(46) Wang, Q. F.; Fan, H. C.; Zhou, Q.; Chen, X.; Wang, L. J.; Lu, Z. X.; Yang, S. X.; Zheng, L. Y.; Cao, Q. E. Reversible Photochromic Coordination Polymer by Phototriggered Subtle Molecular Conformation Variations. *Inorg. Chem.* **2021**, *60*, 18870–18878.
(47) Weerasekara, R. K.; Uekusa, H.; Hettiarachchi, C. V. Multicolor Photochromism of Fulgide Mixed Crystals with Enhanced Fatigue Resistance. *Cryst. Growth Des.* **2017**, *17*, 3040–3047.
(48) Kobayashi, Y.; Abe, J. Recent Advances in Low-Power-Threshold Nonlinear Photochromic Materials. *Chem. Soc. Rev.* **2022**, *51*, 2397–2415.
(49) Yang, B.; Yan, S.; Li, C.; Ma, H.; Feng, F.; Zhang, Y.; Huang, W. Mn(III)-Mediated C–P Bond Activation of Diphosphines: Toward a Highly Emissive Phosphahelicene Cation Scaffold and Modulated Circularly Polarized Luminescence. *Chem. Sci.* **2023**, *14*, 10446–10457.
(50) Saito, T.; Yokozawa, T.; Ishizaki, T.; Moroi, T.; Sayo, N.; Miura, T.; Kumobayashi, H. New Chiral Diphosphine Ligands Designed to Have a Narrow Dihedral Angle in the Biaryl Backbone. *Adv. Synth. Catal.* **2001**, *343*, 264–267.
(51) Jeulin, S.; De Paule, S. D.; Ratovelomanana-Vidal, V.; Genêt, J. P.; Champion, N.; Dellis, P. Difluorphos, an Electron-Poor Disphosphane: A Good Match between Electronic and Steric Features. *Angew. Chem. Int. Ed.* **2004**, *43*, 320–325.
(52) Shimizu, H.; Nagasaki, I.; Matsumura, K.; Sayo, N.; Saito, T. Developments in Asymmetric Hydrogenation from an Industrial Perspective. *Acc. Chem. Res.* **2007**, *40*, 1385–1393.
(53) Genet, J.-P.; Ayad, T.; Ratovelomanana-Vidal, V. Electron-Deficient Diphosphines: The Impact of DIFLUORPHOS in Asymmetric Catalysis. *Chem. Rev.* **2014**, *114*, 2824–2880.
(54) Chen, C.; Chi, Z.; Chong, K. C.; Batsanov, A. S.; Yang, Z.; Mao, Z.; Yang, Z.; Liu, B. Carbazole Isomers Induce Ultralong Organic Phosphorescence. *Nat. Mater.* **2021**, *20*, 175–180.
(55) Wan, H.; Xue, H.; Ling, Y.; Qiao, Y.; Chen, Y.; Zhou, G. Electron Donor and Acceptor Functionalized Dithienylethenes: Effects of Charge Density on Photochromic Properties. *Phys. Chem. Chem. Phys.* **2018**, *20*, 14348–14356.
(56) Abe, M. Diradicals. *Chem. Rev.* **2013**, *113*, 7011−7088.
(57) Alam, P.; Cheung, T. S.; Leung, N. L. C.; Zhang, J.; Guo, J.; Du, L.; Kwok, R. T. K.; Lam, J. W. Y.; Zeng, Z.; Phillips, D. L.; Sung, H. H. Y.; Williams, I. D.; Tang, B. Z. Organic Long-Persistent Luminescence from a Single-Component Aggregate. *J. Am. Chem. Soc.* **2022**, *144*, 3050–3062.
(58) Alam, P.; Leung, N. L. C.; Liu, J.; Cheung, T. S.; Zhang, X.; He, Z.; Kwok, R. T. K.; Lam, J. W. Y.; Sung, H. H. Y.; Williams, I. D.; Chan, C. C. S.; Wong, K. S.; Peng, Q.; Tang, B. Z. Two Are Better Than One: A Design Principle for Ultralong-Persistent Luminescence of Pure Organics. *Adv. Mater.* **2020**, *32*, 1–7.
(59) Chen, Z. X.; Li, Y.; Huang, F. Persistent and Stable Organic Radicals: Design, Synthesis, and Applications. *Chem* **2021**, *7*, 288–332.
(60) Donnay, J. D. H.; Harker, D. A New Law of Crystal Morphology Extending the Law of Bravais. Am. Mineral. 1937, 22, 446−467.
(61) Li, C. Y.; Xu, H.; Cheng, P. M.; Du, M. H.; Long, L. S.; Zheng, L. S.; Kong, X. J. From Helices to Crystals: Multiscale Representation of Chirality in Double-Helix Structures. *J. Am. Chem. Soc.* **2023**.
(62) Zhu, W.; Zheng, R.; Zhen, Y.; Yu, Z.; Dong, H.; Fu, H.; Shi, Q.; Hu, W. Rational Design of Charge-Transfer Interactions in Halogen-Bonded Co-Crystals toward Versatile Solid-State Optoelectronics. *J. Am. Chem. Soc.* **2015**, *137*, 11038–11046.
(63) Liang, X.; Luo, X. F.; Yan, Z. P.; Zheng, Y. X.; Zuo, J. L. Organic Long Persistent Luminescence Through In Situ Generation of Cuprous(I) Ion Pairs in Ionic Solids. *Angew. Chem. Int. Ed.* **2021**, *60*, 24437–24442.
(64) Song, X.; Lu, G.; Man, Y.; Zhang, J.; Chen, S.; Han, C.; Xu, H. Phosphine-Manipulated p-π and π-π Synergy Enables Efficient Ultralong Organic Room-Temperature Phosphorescence. *Angew. Chem. Int. Ed.* **2023**, *62*, e202300980.
(65) Zhao, J.; Wu, W.; Sun, J.; Guo, S. Triplet Photosensitizers: From Molecular Design to Applications. *Chem. Soc. Rev.* **2013**, *42*, 5323–5351.
(66) She, P.; Duan, J.; Lu, J.; Qin, Y.; Li, F.; Liu, C.; Liu, S.; Ma, Y.; Zhao, Q. Single-Component Molecular Dual Persistent Room Temperature Phosphorescence from Low- and High-Lying Triplet States. *Adv. Opt. Mater.* **2022**, *10*, 1–9.
(67) Gao, W.; Dai, X.; Hou, C.; Sun, W.; Gong, Q.; Chen, H.; Ge, Y. Propeller Ultralong Room Temperature Phosphorescence: New Aspect of Triphenylphosphine Derivatives. *Adv. Opt. Mater.* **2023**, *11*, 1–7.
(68) Ma, K.; Chen, W.; Jiao, T.; Jin, X.; Sang, Y.; Yang, D.; Zhou, J.; Liu, M.; Duan, P. Boosting the Circularly Polarized Luminescence of Small Organic Molecules via Multi-Dimensional Morphology Control. *Chem. Sci.* **2019**, *10*, 6821–6827.
(69) Liu, M.; Zhang, L.; Wang, T. Supramolecular Chirality in Self-Assembled Systems. *Chem. Rev.* **2015**, *115*, 7304–7397.
(70) Abdurahman, A.; Hele, T. J. H.; Gu, Q.; Zhang, J.; Peng, Q.; Zhang, M.; Friend, R. H.; Li, F.; Evans, E. W. Understanding the Luminescent Nature of Organic Radicals for Efficient Doublet Emitters and Pure-Red Light-Emitting Diodes. *Nat. Mater.* **2020**, *19*, 1224–1229.
(71) Ai, X.; Evans, E. W.; Dong, S.; Gillett, A. J.; Guo, H.; Chen, Y.; Hele, T. J. H.; Friend, R. H.; Li, F. Efficient Radical-Based Light-Emitting Diodes with Doublet Emission. *Nature* **2018**, *563*, 536–540.
(72) Wang, M.; Zhao, E.; He, Z. Chiral and Luminescent Organic Radicals. *ChemPhotoChem* **2023**, *202300101*, 1–5.
(73) Mayorga Burrezo, P.; Jiménez, V. G.; Blasi, D.; Ratera, I.; Campaña, A. G.; Veciana, J. Organic Free Radicals as Circularly Polarized Luminescence Emitters. *Angew. Chem. Int. Ed.* **2019**, *58*, 16282–16288.

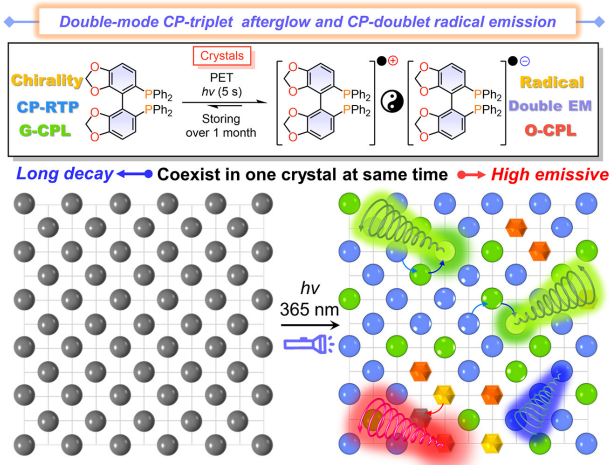

TOC: Double-mode CP-triplet afterglow and CP-doublet radical emission from Janus SEGPHOS crystals